PNAS

Supporting Information for
Structural basis of V-ATPase V_O region assembly by Vma12p, 21p, and 22p

Hanlin Wang, Stephanie A. Bueler, John L. Rubinstein

John L. Rubinstein
Email: john.rubinstein@utoronto.ca

This PDF file includes:

Figures S1 to S9
Tables S1 to S2
Legend for Movie S1
Legend for Dataset S1

Other supporting materials for this manuscript include the following:

Movie S1
Dataset S1

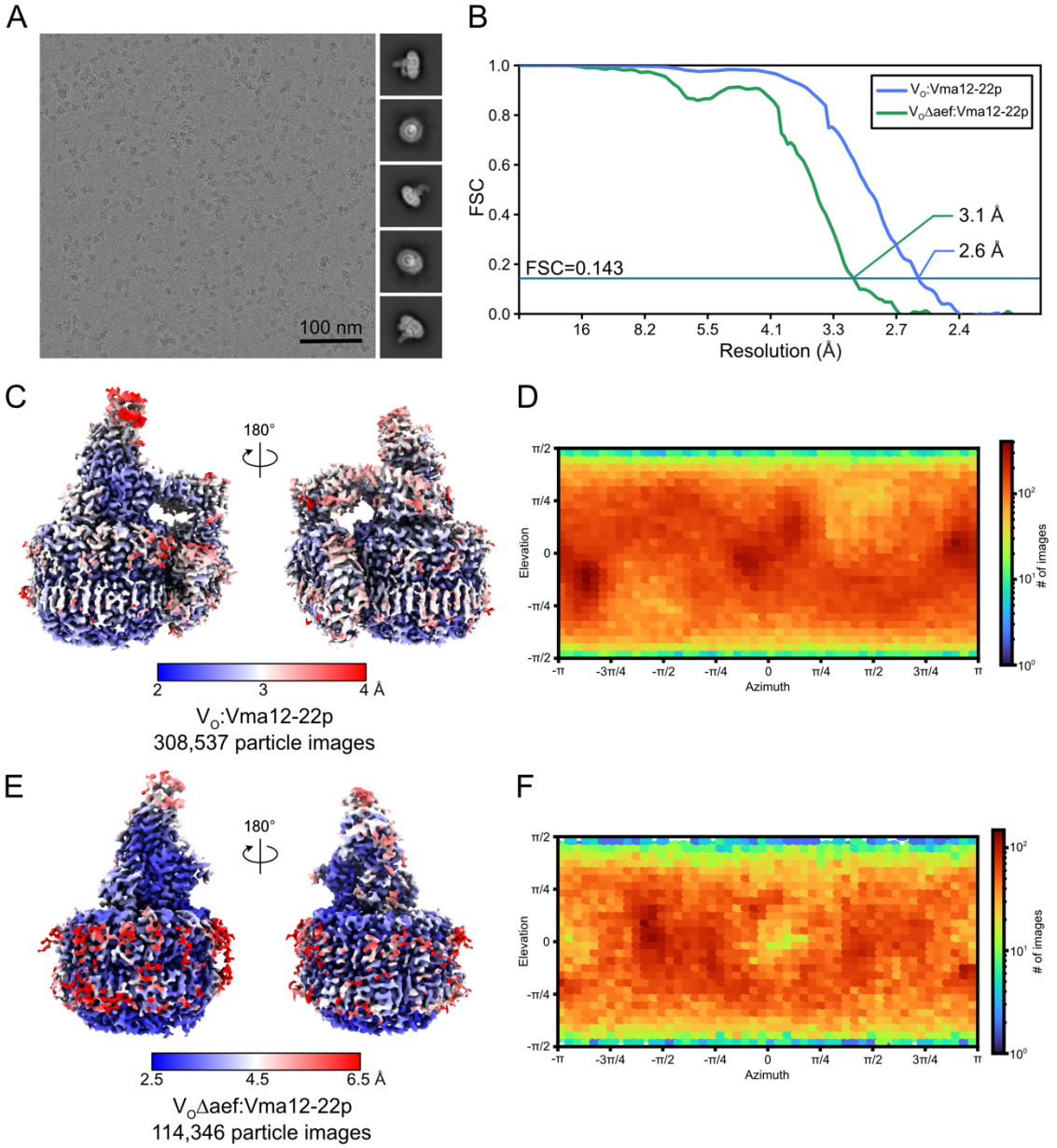

Fig. S1. CryoEM of the V$_O$:Vma12-22p complex. A, Example micrograph and 2D class average images. **B,** Fourier shell correlation curves, corrected for masking, after gold-standard refinement for V$_O$:Vma12-22p and V$_O$Δaef:Vma12-22p. **C,** Local resolution map for V$_O$:Vma12-22p. **D,** Orientation distribution plot for V$_O$:Vma12-22p. **E,** Local resolution map for V$_O$Δaef:Vma12-22p. **F,** Orientation distribution plot for V$_O$Δaef:Vma12-22p.

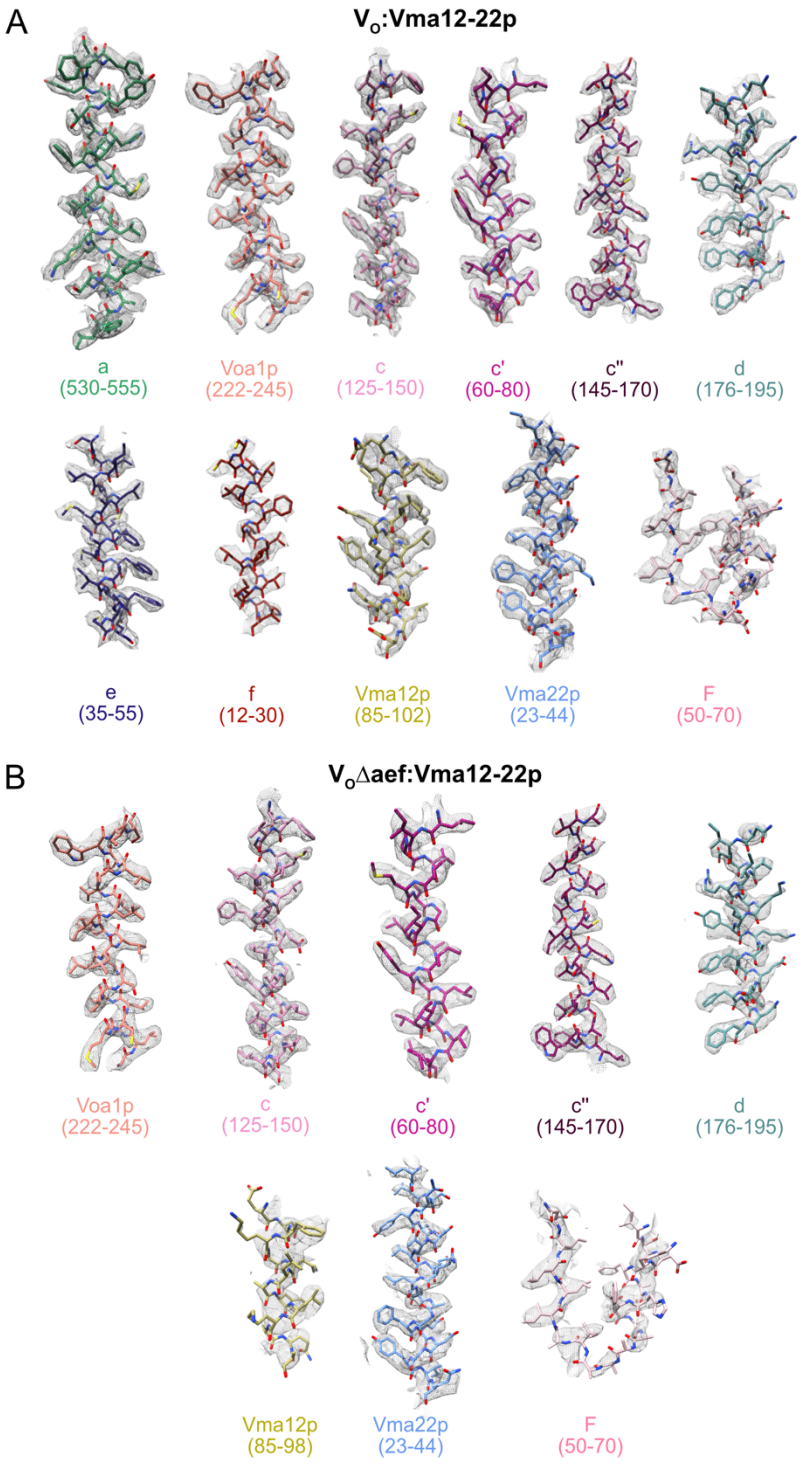

Fig. S2. Model-in-map fit examples. Examples of the atomic model fit in the cryoEM map of V_O:Vma12-22p (**A**) and V_OΔaef:Vma12-22p (**B**).

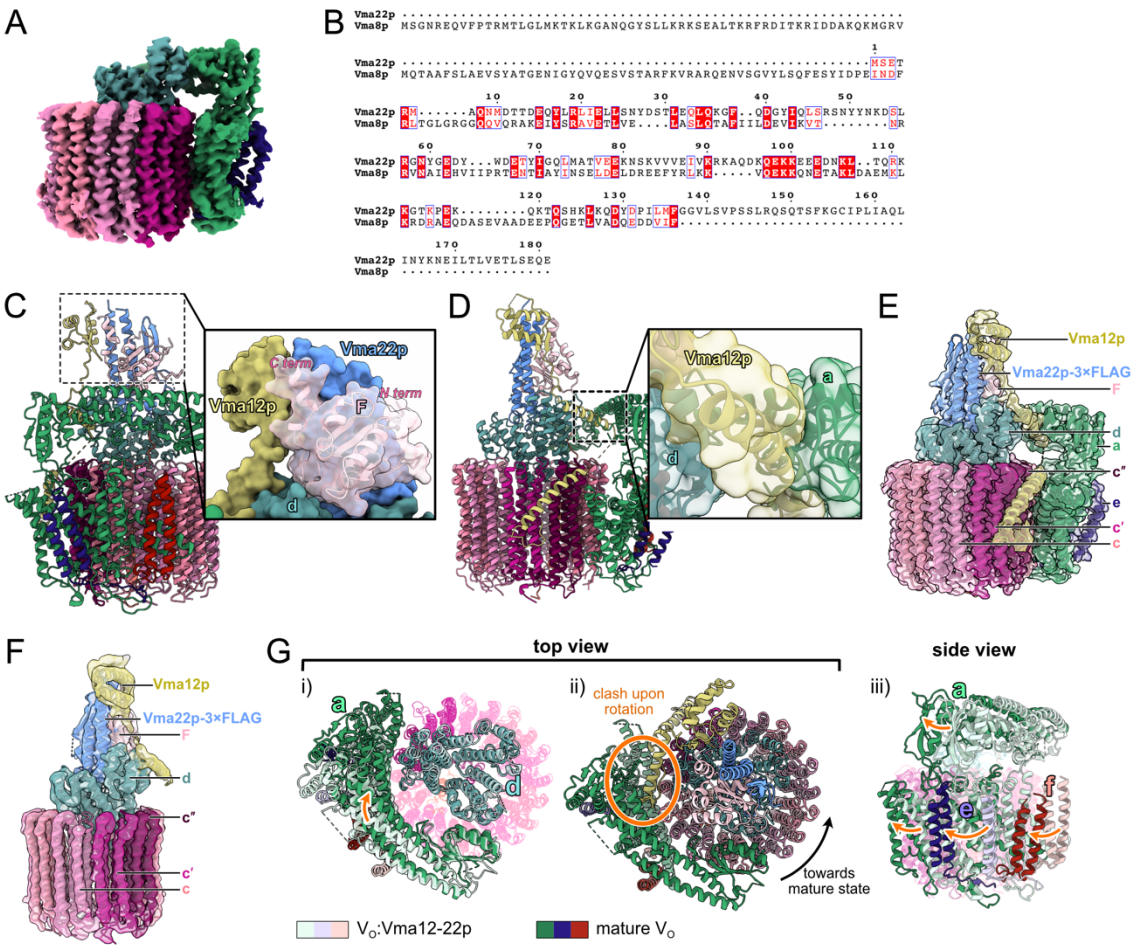

Fig. S3. Structural features of the Vma12-22p complex. A, Re-analysis of a published data of V_O images does not reveal $V_O\Delta$aef complexes. **B,** Protein sequence alignment between Vma22p and Vma8p (subunit D from V_1 complex). Red boxes indicate identical residues and white boxes indicate similar residues. **C,** Subunit F binds Vma12p and Vma22p and mediates their association. **D,** Vma12p interacts with subunits a and d through an α helix. **E,** CryoEM map of V_O:Vma12-22p from the Vma22p-3×FLAG preparation with a model of V_O:Vma12-22p from Vma12p-3×FLAG fitted. **F,** CryoEM map of $V_O\Delta$aef:Vma12-22p from the Vma22p-3×FLAG preparation with a model of V_O:Vma12-22p from Vma12p-3×FLAG fitted. **G,** Movement of subunits a, e, and f relative to the c ring when the c ring transitions to its orientation in the mature V_O complex.

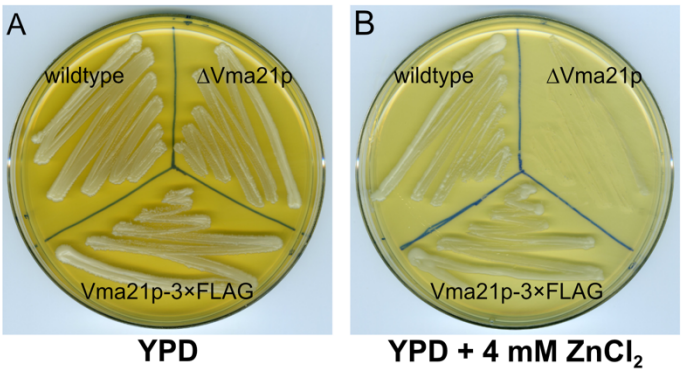

Fig. S4. Integration of a 3×FLAG tag to Vma21p does not compromise V-ATPase function. Comparison of yeast growth for wildtype, ΔVma21p, and Vma21p-3×FLAG yeast strains on YPD (**A**), and YPD with 4 mM of $ZnCl_2$ (**B**). Deletion of Vma21p produces a *VMA*$^-$ V-ATPase deficiency phenotype but addition of a C-terminal 3×FLAG tag to Vma21p does not cause the phenotype.

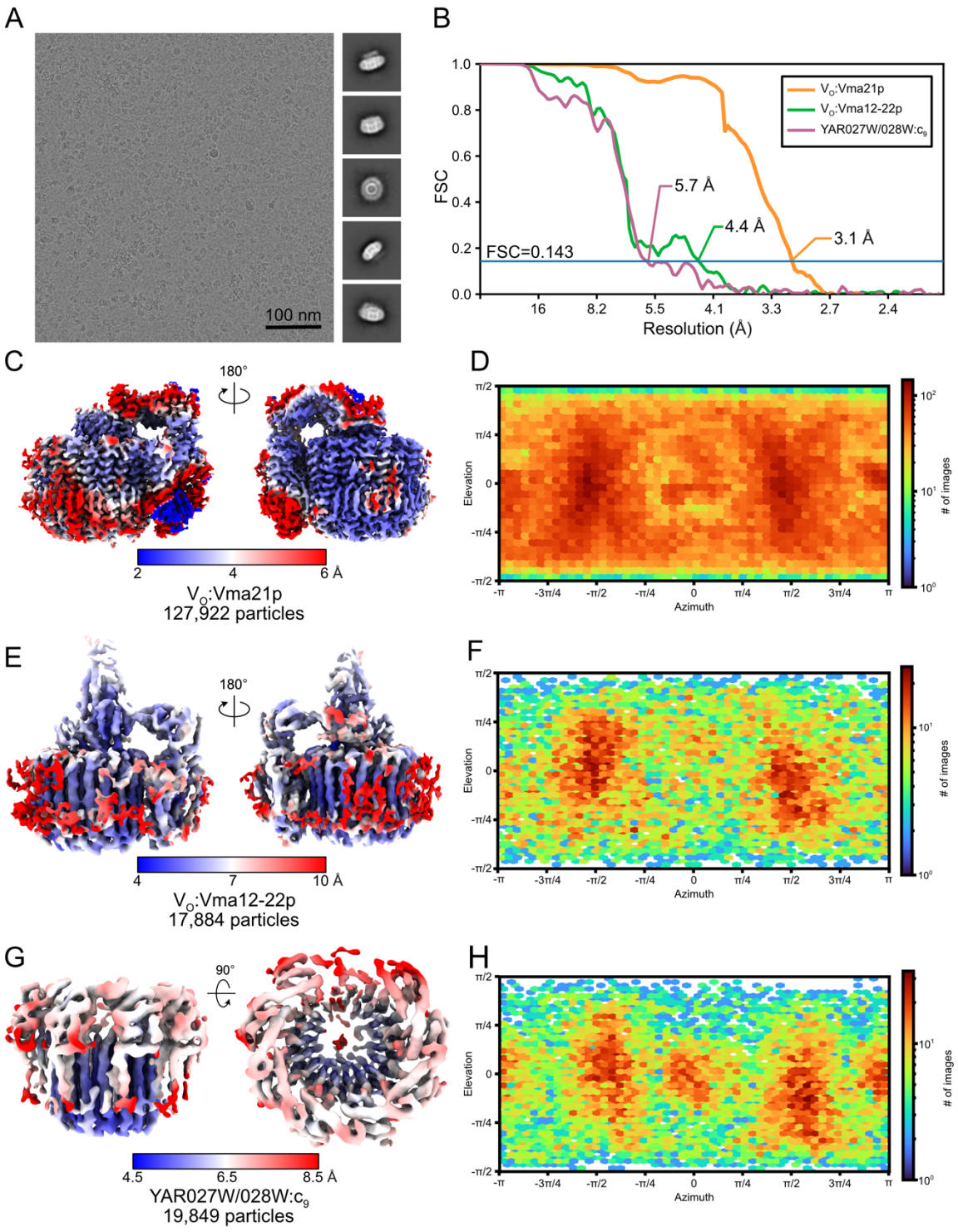

Fig. S5. CryoEM of the Vma21p-3×FLAG preparation. A, Example micrograph and 2D class average images. **B,** Fourier shell correlation curves, corrected for masking, after gold-standard refinement for V_O:Vma21p, V_O:Vma12-22p, and YAR027W/028W:c_9. **C,** Local resolution map for V_O:Vma21p. **D,** Orientation distribution plot for V_O:Vma21p. **E,** Local resolution map for V_O:Vma12-22p. **F,** Orientation distribution plot for V_O:Vma12-22p. **G,** Local resolution maps for YAR027W/028W:c_9. **H,** Orientation distribution plot for YAR027W/028W:c_9.

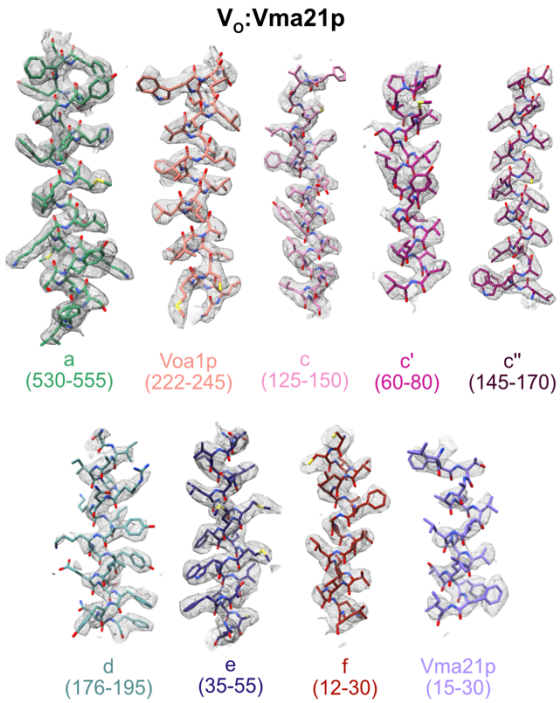

Fig. S6. Model-in-map fit examples. Examples of the atomic model fit in the cryoEM map of V_O:Vma21p.

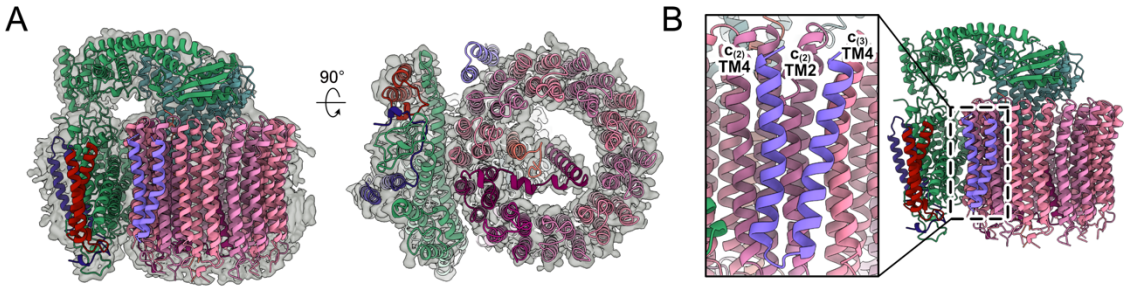

Fig. S7. Comparison of the structure of V_O:Vma21p complex and mature V_O. A, Fitting of the V_O:Vma21p model into the previously-determined V_O map (EMDB: 0644). **B,** Binding location of Vma21p on the c ring.

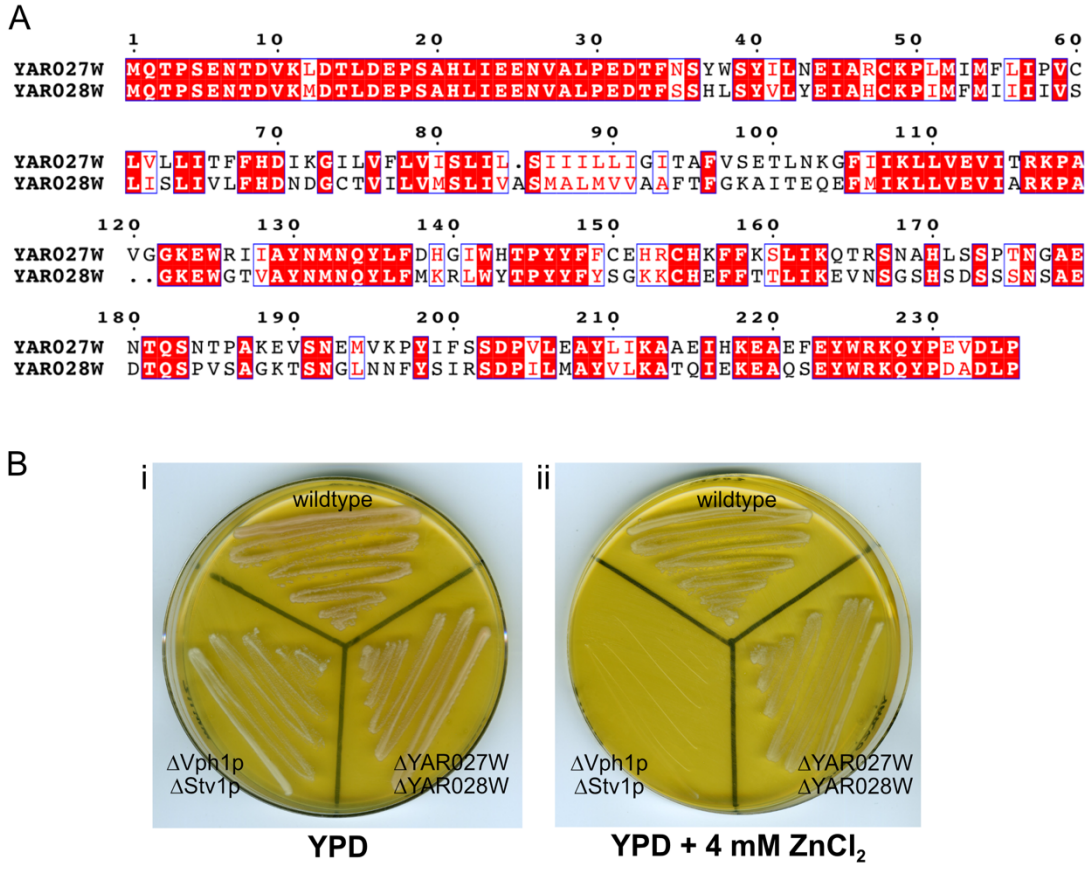

Fig. S8. YAR027W and YAR028W. A, Protein sequence alignment between YAR027W and YAR028W. Red boxes indicate identical residues and white boxes indicate similar residues. **B,** Comparison of yeast growth for wildtype, ΔVph1pΔStv1p, and ΔYAR027WΔYAR028W yeast strains on YPD (**i**), and YPD with 4 mM of $ZnCl_2$ (**ii**). Simultaneous deletion of YAR027W and YAR028W does not cause the *VMA*$^-$ V-ATPase deficiency phenotype, which is seen in the ΔVph1pΔStv1p strain used as a positive control.

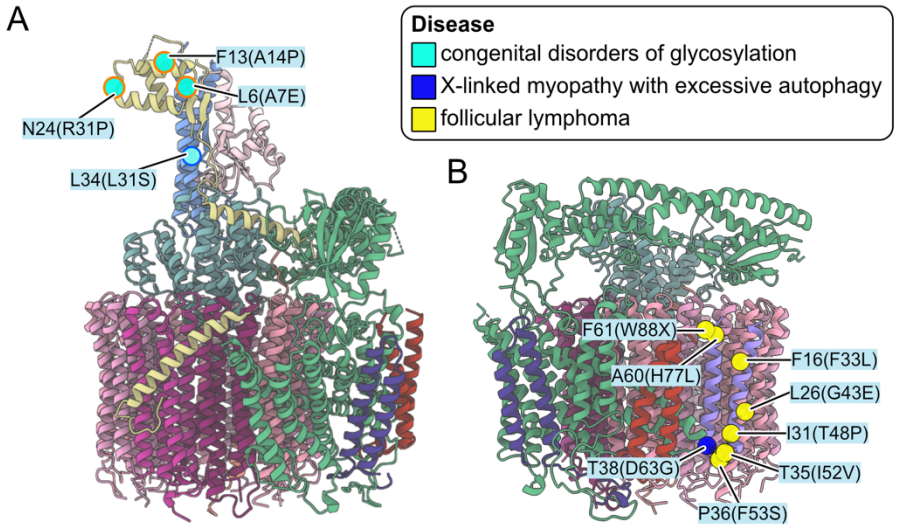

Fig. S9. Disease-associated mutations in human TMEM199, VMA21, and CCDC115 that map onto yeast Vma12p, Vma21p, and Vma22p. A, Mutations of TMEM199 and CCDC115 associated with congenital disorders of glycosylation that map onto yeast Vma12p and Vma22p. **B,** Mutations of VMA21 associated with X-linked myopathy with excessive autophagy and follicular lymphoma that map onto yeast Vma21p. Yeast residues are indicated with disease causing human mutations in brackets.

Table S1. CryoEM map calculation and atomic model construction statistics.

	V_O:Vma12-22p (EMD-27984, PDB 8EAS)	**V_OΔaef:Vma12-22p** (EMD-27985, PDB 8EAT)	**V_O:Vma21p** (EMD-27986, PDB 8EAU)	**YAR027W/028W:c_9 (from Vma21p dataset)** (EMD-27987, PDB 8EAV)	**V_O:Vma12-22p (from Vma21p dataset)** (EMD-27988)
Data collection & Processing					
Magnification	75,000	75,000	75,000	75,000	75,000
Voltage (kV)	300	300	300	300	300
Electron exposure (e^-/Å^2)	45	45	49	49	49
Exposure rate (e^-/pixel/s)	6.7	6.7	6.3	6.3	6.3
Exposure time (s)	7.2	7.2	8.3	8.3	8.3
Defocus range (μm)	0.5-2	0.5-2	0.5-2	0.5-2	0.5-2
Pixel size (Å)	1.03	1.03	1.03	1.03	1.03
Symmetry imposed	C1	C1	C1	C1	C1
Initial particle images (no.)	462,692	462,692	607,746	607,746	607,746
Final particle images (no.)	308,537	114,346	127,922	19,849	17,884
Map resolution (Å)	2.6	3.1	3.1	5.7	4.4
FSC threshold	0.143	0.143	0.143	0.143	0.143
Map resolution range (Å)	2.3-4.8	2.6-6.1	2.2-7.5	4.6-9.2	3.9-11.5
Refinement					
Initial model used (PDB code)	6O7T	6O7T	6O7T	6O7T	
Model resolution (Å)	2.7	3.2	3.2	6.3	
FSC threshold	0.5	0.5	0.5	0.5	
Map sharpening *B* factor (Å^2)	locally sharpened	locally sharpened	locally sharpened	Locally sharpened	
Model composition					
Non-hydrogen atoms	24810	17204	21919	14467	
Protein residues	3280	2349	2946	2890	
Ligands	0	0	0	0	
R.m.s deviations					
Bond lengths (Å)	0.006	0.004	0.004	0.015	
Bond angles (°)	0.635	0.546	0.636	2.359	
Validation					
MolProbity score	1.48	1.45	1.48	2.73	
Clashscore	8.92	5.83	9.07	44.32	
Poor rotamers (%)	0.00	0.00	0.00	0.00	
Ramachandran plot					
Favored (%)	98.61	97.28	98.35	87.78	
Allowed (%)	1.39	2.72	1.65	8.38	
Disallowed (%)	0.00	0.00	0.00	3.84	

Table S2. DNA primers used for strain construction and confirmation.

Yeast strain	forward primer with plasmid pJT1	reverse primer with plasmid pJT1	forward confirmation primer	reverse confirmation primer
SABY125 (Vma12p-3×FLAG)	5′-AAGAAAAA CAAAGGTTGAGAAAAAGA AAGTTCTAAGCAAGATTA CACTGGACTACAAAGACC ATGACGG-3′	5′-AAGAATTAT ATGCTCTCGGATCTCGGA GTTCTTATTTATAAAATG ATCAGATATCATCGATGA ATTCGAGCTCG-3′	(5′ junction) 5′-GCCATT TGGTACTGGACCGG-3′	(5′ junction) 5′-GAGCGA CCTCATACTATACC-3′
SABY129 (Vma21p-3×FLAG)	5′-TCCGCGAGGATACTGAAG ATCACAAAGTTGATGGTA ATAAAAAGGAAGACGACT ACAAAGACCATGACGG-3′	5′-CCTCTACTA TTTTTCTTGTATATTCTC TTCTAGCAACATATACTA CTCAAATATCATCGATGA ATTCGAGCTCG-3′	(5′ junction) 5′-GTAGAT GTTCCTCGTGCGGTG-3′	(5′ junction) 5′-GAGCGA CCTCATACTATACC-3′
SABY130 (Vma22p-3×FLAG)	5′-ATTACAAGA ACGAAATATTAACGTTGG TTGAAACGTTGTCTGAGC AGGAAGACTACAAAGACC ATGACGG-3′	5′-CTTCAAATA TACACGTATGTATTATTT CTTTTTACTATATTCTTA ACTCTATATCATCGATGA ATTCGAGCTCG-3′	(5′ junction) 5′-TGGTGG AGTACTGTCCGTTCC-3′	(5′ junction) 5′-GAGCGA CCTCATACTATACC-3′
SABY149 (ΔYAR027W ΔYAR028W)	5′-ACCTCCAAA ACCATATAATAACCTTAC ACAAGACAAGATATCAAT TCAACGGCGCGCCACTTC TAAATAAGC-3′	5′-TCTCGTTTT AAAGAAAAGTAAGTATAC TTGGTGAATAAAATGCTT CCGCTATATCATCGATGA ATTCGAGCTCG-3′	(5′ junction) 5′-AAAGCT CAATTAGTATCATGATC-3′ (3′ junction) 5′-CGACAT CATCTGCCCAGATG-3′	(5′ junction) 5′-GAGCGA CCTCATACTATACC-3′ (3′ junction) 5′-GATGCT CAATTCTGGCTTCG-3′

Movie S1 (separate file). Movie S1. Model for the sequence of events in V_O assembly.

Dataset S1 (separate file). Mass spectrometry identification of proteins purified with Vma21p-3×FLAG preparation.